

Which are the youngest protostars?

Determining properties of confirmed and candidate Class 0 sources by broad-band photometry

D. Froebrich

Dublin Institute for Advanced Studies, 5 Merrion Square, Dublin 2, Ireland

ABSTRACT

We searched the literature to obtain a complete list of known Class 0 sources. A list of 95 confirmed or candidate objects was compiled. To the best of our knowledge, all published broad-band observations from $1\text{ }\mu\text{m}$ to 3.5 mm have been collected and are assembled in a catalogue. These data were used to determine physical properties (T_{bol} , L_{bol} , $L_{\text{smm}}/L_{\text{bol}}$, M_{env}) and for a uniform classification. 50 sources possess sufficient observational data and are classified as Class 0 or Class 0/1 objects. The source properties are compared with different evolutionary models to infer ages and masses, and their correlations are investigated. About 25% of the sources are found to be in a quiet accretion phase or possess a significantly different time evolution of the accretion rate than the average. In Taurus, with its isolated star formation mode, this seems especially to be the case.

Subject headings: Catalogs – Stars: evolution – Stars: formation – Infrared: stars

1. Introduction

Protostars begin their life soon after the collapse of their parental cloud core begins. Such stellar embryos have masses of less than $10^{-2} M_{\odot}$ (Larson (2003)) and are deeply embedded in a dense and massive envelope of gas and dust. The central object grows in mass by accreting material from this envelope either by direct infall or via a flattened circumstellar disc. As long as the central object is less massive than the surrounding envelope it is called a Class 0 object. Otherwise it is a Class 1 protostar. Since this mass ratio is not directly observable, other criteria have to be adopted for a classification. André et al. (2000) defined three observational properties needed to classify an object as a Class 0 source: (i) an internal heating source (compact centimeter radio continuum) or bipolar outflow as an indication of a central young stellar object; (ii) extended and centrally peaked sub-millimeter continuum emission, indicating the spheroidal envelope; (iii) a high ratio of sub-millimeter to bolometric luminosity ($L_{\text{smm}}/L_{\text{bol}} > 0.005$), with L_{smm} measured longward of $350\text{ }\mu\text{m}$. It is shown in André et al. (1993) that this last criterion is equivalent to the mass ratio of the envelope and the central star being larger than one.

Other authors use the bolometric temperature (T_{bol}) instead of $L_{\text{smm}}/L_{\text{bol}}$ (e.g. Chen et al. (1995a; 1997) use $T_{\text{bol}} < 70\text{ K}$).

The Class 0 stage can be characterised as the main mass accretion phase, in which the forming star gains the bulk of its final mass. This process is not yet well understood. How does the mass accretion rate depend on the age and the properties of the cloud, and is it governed by turbulence or ambipolar diffusion? What is the lifetime of the Class 0 sources? How are the source properties connected to the molecular outflow, that is inevitably driven by these objects? The answers to these questions will finally help us to understand the feedback of the star formation process to the surrounding molecular cloud and the initial mass function.

To seriously address these questions we need a large, homogeneously classified sample of these very young protostellar objects. Several samples have been compiled in the recent years (e.g. Chen et al. (1995a), André et al. (2000), Shirley et al. (2000), Motte & André (2001)). All these works have specific problems: (1) they concentrate only on a limited number of sources; (2) different criterias for classification of Class 0 objects are used; (3) only parts of the available

observational data are considered.

The first step to obtain a large, homogeneously classified sample of Class 0 sources is a complete search of the literature for such objects. Here we present an as far as possible complete list of the youngest known protostars to date. We will classify them by means of their spectral energy distribution (SED) using all (to the best of our knowledge) published broad-band photometric data. We derive basic properties of these sources (T_{bol} , L_{bol}). The sub-mm data are used to estimate envelope masses (M_{env}) and sub-mm slopes of the SED (β). By comparing T_{bol} , L_{bol} , and M_{env} with evolutionary models we determine ages and masses of these sources and investigate limitations of the current observational data and evolutionary models. This is of particular interest for forthcoming powerful telescopes like Spitzer and ALMA, which will enable us to improve our knowledge of these sources significantly. Given this expected growth in observational data in the near future, the present catalogue might be quickly outdated. Hence, all the data will be available on a webpage¹ and updated regularly.

In Sect. 2 we introduce the source sample. The method of our data analysis is then put forward in Sect. 3, including a description of the source classification in Sect. 3.2. Finally the results and implications are discussed in Section 4.

2. Source sample and broad band photometry

To obtain an as far as possible complete list of known Class 0 objects we combined the samples of candidates and sources mentioned in various publications. In particular we combined: (1) sources with $T_{\text{bol}} < 100$ K from Chen et al. (1995a); (2) objects with $T_{\text{dust}} < 100$ K from Hurt et al. (1996); (3) Class 0 sources listed in Bontemps et al. (1996); (4) objects of type CL0 in Saraceno et al. (1996); (5) candidates with $T_{\text{bol}} < 100$ K from Chen et al. (1997); the source B 35 could not be identified in SIMBAD; (6) Objects with $L_{\text{bol}}/L_{\text{smm}} < 200$ in Chini et al. (1997a) with VLA detected counterparts in Reipurth et al. (1999); (7) the Class 0 sources in CB 68 and CB 232 mentioned in Huard et al. (1999); (8) objects classified as Class 0 in Park et al. (1999); (9) all objects listed in André et al. (2000); (10) Class 0 sources in Shirley et al. (2000); (11) sources indicated as Class 0 or Class 0/1 in Motte & André (2001); (12) objects with

$L_{\text{FIR}}/L_{\text{smm}} < 200$ in Chini et al. (2001); (13) candidates with $T_{\text{bol}} < 100$ K in Lehtinen et al. (2001); (14) Class 0 sources from Visser et al. (2002); (15) objects with $T_{\text{bol}} < 100$ K listed in Young et al. (2003); (16) Class 0 objects and candidates investigated in Froebrich et al. (2003); (17) candidates and confirmed Class 0 sources from Rengel et al. (2004); (18) the possible Class 0 sources NGC 7129 FIRS2 (Eiroa et al. (1998)), NGC 2068 LBS 17 (Gibb & Little (2000)), IC 348 MMS (Eislöffel et al. (2003)), NGC 7538 S (Sandell et al. (2003)), and MonOB1 IRAS12 S1 (Wolf-Chase et al. (2003)). All investigated sources with their positions, adapted distances, and references are listed in Appendix A in Table 3. This table will be only available in electronic form and lists the object name used in this paper and other common names of the sources.

Sources in the combined sample were identified by their position in the SIMBAD database in order to avoid confusion due to unclear or conflicting nomenclature. A search in the related publications given by SIMBAD for the sources was performed and to our best knowledge all available broad-band photometric data were extracted. We restricted the search for data ranging from the near infrared (NIR) to wavelengths shorter than 3.5 mm. At longer wavelengths the emission of the envelope might be a combination of dust continuum and free-free emission from the central source and may influence the analysis of the envelope properties. NIR and mid-infrared detections with brightness given in magnitudes were converted into Jansky using flux zero-points of Wamsteker (1981). In case of non-existing NIR detections in the literature we searched the 2MASS catalogue. If the source was not detected by 2MASS, we determined an upper limit (the faintest flux in the 2MASS catalogue within 200'' of the source).

3. Data analysis

3.1. Basic parameters

The observed SEDs have to be characterised in order to be able to compare them and learn about the object properties. We computed T_{bol} following the method described in Chen et al. (1995a). This is the temperature of a black body, which possesses the same mean frequency as the respective source. The bolometric luminosity is determined by integrating the SED and adapting a distance. Note that L_{bol} might be underestimated by this method, when the emission

¹<http://www.dias.ie/protostars>

maximum is not well covered (no data from 100 to 350 μm). We compute the ratio of bolometric to sub-mm ($\lambda > 350 \mu\text{m}$) luminosity. This ratio is used in the source classification (see Sec. 3.2).

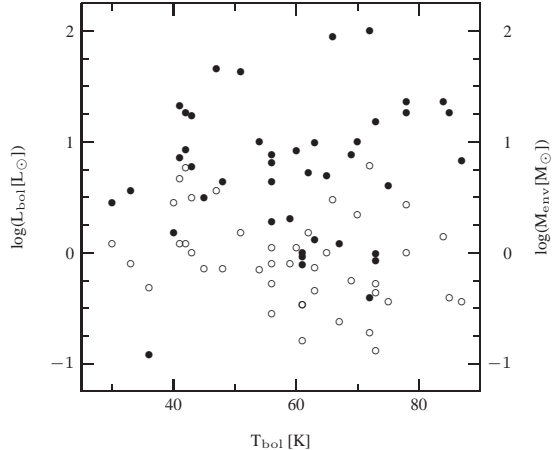
The mean spectral index α was determined by a powerlaw fit to fluxes measured longward of 400 μm . α is converted to the powerlaw index of the dust emissivity (assuming optically thin emission) by $\beta = \alpha - 2$. The powerlaw fit allows for a uniform determination of the flux density at 1.3 mm, even if the object was not observed at this wavelength. The fluxes are scaled to a distance of 300 pc and transformed into envelope masses by $M_{\text{env}} = 1.5 M_{\odot} * F_{1.3\text{mm}}^{300\text{pc}} [\text{Jy}]$ (following Motte and André (2001)). We used a dust opacity at 1.3 mm of 0.01 $\text{cm}^2 \text{g}^{-1}$ and a dust temperature of 24 K for all objects. A lower dust temperature of 15 K, as e.g. suggested by Motte & André (2001) for the Taurus sources, would lead to envelope masses which are a factor of 1.6 higher.

The data for some sources are inhomogeneous. Different aperture sizes are used at different wavelengths. To ensure a consistent treatment of the data for all sources, datapoints were selected or excluded manually before the determination of the source properties. In Table 4 (Appendix B, available online only) we list datapoints not used for the determinations, together with further notes. The obtained parameters for all our sources are listed in Table 1. This table is divided in three sections. First we list all sources where the SED is very well sampled and all parameters can be determined accurately. The second part contains sources where the SED is only well determined on one side of the peak and for the other side only upper limits (e.g. VLA 1623) or very few data (e.g. CB 232) are available, hence mostly limits for the source properties could be derived. In the last part we list sources that have very insufficient data and where at best only β and M_{env} or a lower limit for L_{bol} can be determined. The objects Trifid-TC 3, GF 9-2, and IC 348 MMS are not listed in this table since none of the source properties could be determined.

3.2. Source Classification

To classify the investigated objects we conducted three different tests for objects listed in the first two parts of Table 1. A source was negatively tested to be a Class 0 object when: (1) T_{bol} is larger than 80 K; (2) $L_{\text{smm}}/L_{\text{bol}}$ is less than 0.005; (3) There is a NIR ($\lambda < 5 \mu\text{m}$) detection. If all three tests are positive then

Fig. 1.— Distribution of L_{bol} (filled circles) and M_{env} (open circles) against T_{bol} of the Class 0 and Class 0/1 sources with distances of less than 500 pc.



the source was marked as Class 0 object (0). If at least two tests are positive and the third could not be conducted or was negative, then the source is marked as borderline object (0/1). In case of two negative tests the source is classified as Class 1 (1). For all remaining objects a classification cannot be performed and the source is marked by '?'. In principle we further need to test if the object possesses an extended envelope. Hence, we marked all sources with a † symbol, where non or no conclusive sub-mm or millimeter map is available. The lack of such data mostly effects southern hemisphere objects, which anyway could not be properly classified by our tests.

The classification obtained for each source according to these criteria is listed in the last column of Table 1. Positions in the $T_{\text{bol}}-L_{\text{bol}}$ diagram of all sources properly classified as Class 0 or Class 0/1 can be seen in Fig. 1 together with the $T_{\text{bol}}-M_{\text{env}}$ positions. In order to obtain a well defined sample with as few as possible selection effects, we excluded sources with distances larger than 500 pc in the diagram.

3.3. Evolutionary Models

Bolometric temperature, luminosity and envelope mass are three observational quantities available for these young sources. To investigate physical properties, such as final masses and ages, we need to compare these values with evolutionary models. For the comparison we selected all sources from part one in Table 1 and the objects from part two with a clear classification (0, 0/1, or 1), and where T_{bol} , L_{bol} , and M_{env}

could be determined.

There are several evolutionary schemes available in the literature. We use three different models to estimate ages and final masses of our sources. (1) The evolutionary diagram presented in Fig. 12 of Myers et al. (1998), where the infall rate matches the isothermal sphere infall solution at early times and exponentially declines later. (2) Evolutionary tracks shown in Fig. 6b in André et al. (2000), where accretion rate and envelope mass decline exponentially. (3) The evolutionary scheme developed by Smith (1998; 2000; 2002), where the mass accretion rate first increases exponentially and then shows a powerlaw fall off.

All of these evolutionary models are subject of shortcommings. They are based on assumptions about the time dependence of the mass accretion rates. While the overall decline with time has substantial observational support (Calvet et al. (2000)), the particular behaviour is unclear. Analytical and numerical models reproduce both, exponential decline (Shu et al. (2004)) or well defined early peaks followed by a fall off (Schmeja & Klessen (2004)). The usage of T_{bol} and L_{bol} as input parameters (Smith (1998; 2000; 2002), Myers et al. (1998)) will lead to uncertainties since both depend on the viewing angle, in contrast to the envelope mass (André et al. (2000)), which is inferred from optically thin dust emission. Hence, the absolute values of the determined ages and masses are model dependent but the relative values can be used to put these youngest known protostars in an evolutionary sequence. Calculated ages and final masses from all models are listed in Table 2.

4. Discussion

4.1. Source classification

We investigated SED's of 95 young protostellar sources. 59 of these objects (60 %) possess sufficient observational data to accurately determine all properties (T_{bol} , L_{bol} , M_{env}). Out of these, 27 objects could be unambiguously classified as Class 0 object, 23 as Class 0/1, and 9 as Class 1 protostars (according to our definition). There is a remaining relatively large number (36 objects; 40 %) where we do not have sufficient information about the SED for a proper classification.

There are two main gaps in the observational data which mean this large fraction could not be classified properly. (1) Only data at wavelengths shorter than the emission maximum and non or only insufficient sub-

mm or millimeter observations are available. Hence, only upper limits for T_{bol} and lower limits for L_{bol} can be determined. (2) Only data at wavelengths longer than the maximum and no observations or just upper limits at shorter wavelengths are available. For these objects only β and M_{env} can be estimated properly.

4.2. Uncertainties

All determined object parameters are subject to different errors, due to their calculation. The powerlaw index of the opacity is determined from the mean slope of the SED at $\lambda > 400 \mu\text{m}$. Using fluxes taken with different aperture sizes to determine β will lead to different results. Estimating β as the mean slope ensures that for each object a 'mean' aperture size for the (sub)mm data is used. Typical errors of the estimated values are 0.3.

The luminosity is determined by integrating the SED and adopting a distance. An error of 20% for the distance (a typically value for most of the objects with $d < 500 \text{ pc}$) leads to 40% uncertainty for the luminosity. Also the luminosity might be underestimated when the SED is not well sampled at the emission peak, or when huge parts of the SED are only described by upper limits (e.g. VLA 1623 or HH 24 MMS). Additional uncertainties are expected in cluster regions, where current far-infrared instruments do not possess sufficient angular resolution to separate individual sources (e.g. SVS 13 B). Non-detections or observations in the NIR or at millimeter wavelength have almost no influence, since most energy is radiated near the emission maximum. All together the determined source luminosities are uncertain by about 50% in most cases.

For the bolometric temperature, datapoints at short wavelengths are important. In the case of well sampled SEDs from the NIR to the sub-mm, T_{bol} can be determined with about 5 to 10 K accuracy. In the case of upper limits in the NIR, the same accuracy applies as long as the limits are at least 5-6 orders of magnitude lower than the flux at the maximum of the emission. Note that the sources classified as Class 0/1 have typically NIR detections 4-5 orders of magnitude below the emission maximum, while for the Class 0 sources we find typical non-detections 5-7 orders of magnitude below the maximum. In case of 'bad' NIR limits the uncertainty in T_{bol} can well exceed 10 K. Hence for our Class 0 sources the temperatures are accurate to 10 K, while for the Class 0/1 objects they are certain to 20 K. Note that for older sources (Class 0/1 or Class 1)

viewing angle effects might become important. They lead in case of edge-on sources to underestimates of T_{bol} and L_{bol} . Subsequently the $L_{\text{smm}}/L_{\text{bol}}$ ratio is overestimated, influencing the source classification.

The envelope mass is also subject of various sources of errors. Beside the problems with measuring the fluxes in different apertures, the distance is used in the determination. Further the applied dust opacities are uncertain by a factor of two (e.g. Motte & André (2001)), and the dust temperatures are not very well known. Hence, the masses might suffer from errors of a factor of three.

How do these errors influence inferred ages and masses? The models of Smith (1998; 2000; 2002) and Myers et al. (1998) use T_{bol} and L_{bol} as main input parameter. In both cases the error in the measured luminosity leads to uncertainties of about a factor of two for the estimated final masses. Errors in T_{bol} will transform into age uncertainties which are about 30%. The model of André et al. (2000) uses the envelope masses as input. Hence inferred final masses are uncertain by a factor of three and estimated source ages are uncertain by a factor of two. Note that these uncertainties do not take into account systematic errors due to the various assumptions made in the different evolutionary models.

4.3. Distribution of source parameters

To investigate the statistical properties of the obtained Class 0 sample, we restrict all the following discussions to sources classified as Class 0 or Class 0/1 objects within 500 pc.

The power-law index of the opacity is evenly distributed from 0.0 to 2.0 with a broad maximum between 0.5 and 1.5. For our sources T_{bol} ranges from 30 to 90 K, where the 90 K limit is due to our classification criterion for Class 0 sources. The number of sources gradually rises from 30 to 70 K and falls off at higher temperatures. One expects a rising (or at least constant) number of sources towards higher temperatures, because with higher temperature an increased age and a slower evolution in temperature is predicted by the models. Hence, the T_{bol} distribution shows that there are missing objects in our sample in this temperature range. This might be due to a classification of these objects as Class 1 protostars and reflect the fact that sources with the same bolometric temperatures are not necessarily in the same evolutionary state. The distribution of L_{bol} corresponds very well with the

mass function (see below), due to the assumptions in the evolutionary models. Similarly the distribution of M_{env} shows a peak at about one solar mass. At lower masses our sample certainly suffers from incompleteness. The $L_{\text{smm}}/L_{\text{bol}}$ ratio shows a broad distribution between 0.01 and 0.1. Only very few larger values are found (IRAM 04191, L 1448 NW).

We further investigated if the source properties are correlated. There is no correlation between the dust opacity β and the parameters T_{bol} and L_{bol} (correlation coefficients (c.c.) -0.034 and -0.102). A weak correlation (c.c. -0.412) is found between β and M_{env} , but this is due to a few high envelope mass sources. Also T_{bol} is not correlated with L_{bol} and M_{env} (c.c. 0.149 and -0.219). On the other hand the envelope mass shows a correlation with the bolometric luminosity (c.c. 0.660). This correlation indicates that objects with more massive envelopes possess a higher luminosity and hence higher accretion rates.

4.4. The different evolutionary models

Due to the different model assumptions about the time evolution of the mass accretion rates, all three investigated evolutionary models lead to different values for ages and final star masses. The ages especially are very model dependent. We investigate if there are correlations between the inferred values for age and final mass for the different evolutionary models in our Class 0 and Class 0/1 sample.

On first sight the ages differ significantly between the models. Ages from Myers et al. (1998) are much larger than usually assumed for Class 0 sources (a couple of 10^4 yrs). In the model of André et al. (2000) the evolution in the first 10000 yrs is very fast, and hence the inferred ages are on average very small ($< 10^4$ yrs). However, there is a weak correlation between the ages inferred from the model of Smith (1998; 2000; 2002) and Myers et al. (1998) (c.c. 0.425). Comparing the models from André et al. (2000) with Myers et al. (1998) and Smith (1998; 2000; 2002) we find no correlation (c.c. 0.143, 0.263).

The predicted final masses are much more important than the ages, since the mass distribution should represent the observed initial mass function. Here we investigate if the relative masses obtained from the different models are comparable. There are no obvious differences in the inferred masses between the models. The models of Myers et al. (1998) and André et al. (2000) are limited in their mass range (0.3-0.7 and

$0.2\text{--}3.0 M_{\odot}$, respectively). We find good correlations between masses obtained from the different models: c.c.=0.676 for Smith (1998; 2000; 2002) and Myers et al. (1998); c.c.=0.656 for Smith (1998; 2000; 2002) and André et al. (2000) and c.c.=0.771 for Myers et al. (1998) and André et al. (2000)).

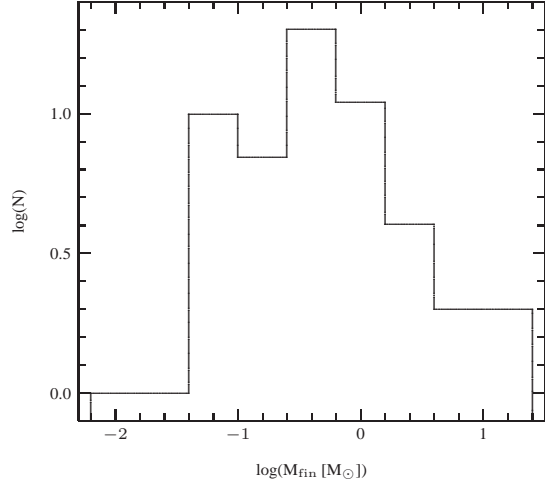
4.5. The Mass Function

The evolutionary scheme by Smith (1998; 2000; 2002) allows the comparison of all three main observational quantities (T_{bol} , L_{bol} , M_{env}) with the model. Also there is no restriction on the final mass as in the other models. Further, the assumed mass accretion rates are very similar to accretion rates obtained by hydrodynamical simulations of star formation (e.g. Klessen (2001), Schmeja & Klessen (2004)). Hence it is worth to investigate the resulting final mass function obtained for our sources using this model. Certainly the absolute values for the masses are uncertain, but giving the good correlations to the other models (see above), the relative masses, needed to determine the slope in the mass function, are correct.

In Fig. 2 we present the resulting mass function for our sample of Class 0 and Class 0/1 objects within 500 pc. The slope determined for objects with $M > 0.5 M_{\odot}$ is -0.9 ± 0.2 . Considering the low number of sources, and that no binary correction is done, this is in good agreement with the Salpeter slope of -1.35 measured for the solar neighborhood. We estimate a completeness limit in our sample for objects with final masses below $0.4 M_{\odot}$.

There is, however, a number of predicted very low mass sources. These are objects where the model of Smith (1998; 2000; 2002) seems not to work properly. Looking in detail, we find that the evolutionary scheme of Smith (1998; 2000; 2002) can explain the all observed properties (T_{bol} , L_{bol} , M_{env}) for most of the sources simultaneously. In case of eleven objects, however, the scheme is not working (IRAS 03256+3055, IRAS 03282+3035, B 213, IRAM 04191, L 1448 N, IRAS 04325+2402, IRAS 04368+2557, IRAS 15398-3359, HH 24 MMS, NGC 2068 LBS 17, VLA 1623). These sources possess a much lower luminosity (considering their T_{bol} and M_{env} values) than the average of the objects. There are also three objects where the luminosity is much above the average (NGC 1333-I2, HH 212-MM, L 1641 N). Note that this applies also for the more distant objects L 1246-SMM 1 (luminosity lower) and

Fig. 2.— Mass Function for the properly classified Class 0 and Class 0/1 objects within 500 pc, obtained from the model of Smith (1998; 2000; 2002).



Cep E, IRAS 20050+2720, and MonOB1 IRAS12 S1 (luminosity higher). For the remaining sources the model explains very well all three observed properties.

There are two reasons for this inability to explain the data of all our objects. (1) One might be found in the mass accretion rates obtained by Klessen (2001) and Schmeja & Klessen (2004). It turns out that their accretion rates on average show a time evolution similar to the one used in the model of Smith (1998; 2000; 2002). But on short timescales the accretion rate varies significantly from this average. There are periods with lower and higher accretion rates resulting in higher and lower luminosities. Hence, the very low luminosity sources might represent a quiet accretion phase, while the higher luminosity sources represent phases of enhanced accretion. (2) A second reason might be that these sources do not accrete their mass in the same way. Hence, the mass accretion rate shows a significantly different evolution in these objects.

In case of the latter, this suggests two different groups of sources. 'Normal' sources, possessing accretion rates similar to that obtained by Schmeja & Klessen (2004), and 'abnormal' sources showing on average lower luminosities/accretion rates, considering their T_{bol} and M_{env} values. Note that viewing angle effects could be responsible for some of these objects. These low luminosity sources might represent objects where ambipolar diffusion dominates the accretion process instead of turbulence. A detailed

analysis and discussion of this subject can be found in Froebrich et al. (2004).

4.6. The different Star Forming Regions

Does the star formation process, in particular the time dependence of the mass accretion rate vary with the star forming region or is it a uniform function? Due to the low number of sources a proper statistical analysis of this question is not possible yet. However, in order to see possible trends we chose four regions (Perseus, Taurus, Orion, and Serpens) where we have a sufficient number of confirmed Class 0 or Class 0/1 objects (13, 4, 10, 6, respectively) and compared these regions with the average of all sources.

In our sample of Class 0 and Class 0/1 sources about 25% do not follow the $T_{\text{bol}}\text{-}L_{\text{bol}}\text{-}M_{\text{env}}$ relation of the majority of our objects. These sources possess much lower luminosities than suggested by their bolometric temperature and envelope mass. Hence, they might be in a phase of lower mass accretion or are gaining their mass in a different way. Perseus reflects the overall average with three out of 13 objects. The same applies for Orion (two out of ten), where we might miss low luminosity objects due to the larger distance. In Serpens all of the six sources show a 'normal' behaviour. This is, according to the small number of objects, still in agreement with the average. Taurus, however, shows a very different picture. Here all four Class 0 or Class 0/1 objects fall into the low luminosity category. Objects showing a 'normal' behaviour should have been easily detected since their higher luminosity. Hence, even if there are just four sources this strongly suggests that in a region of isolated star formation (as in Taurus) the time evolution of the mass accretion rates is different from regions where stars form in clusters (in agreement with previous findings from Henriksen et al. (1997)). Due to the bad statistics nothing can be said about differences among the clusters.

5. Conclusions

A literature search for photometric broadband observations of 95 confirmed or candidate Class 0 sources was conducted. To our best knowledge all available broadband photometric data was used to construct SEDs from $1\text{ }\mu\text{m}$ to 3.5 mm . If possible we determined basic properties of the sources (sub-mm slope of the SED, T_{bol} , L_{bol} , $L_{\text{smm}}/L_{\text{bol}}$, and M_{env}). For 59 objects sufficient enough data are available for

a proper determination of the source parameters. 27 of these are classified as Class 0, 23 as Class 0/1, and 9 as Class 1 protostars.

To investigate the statistical properties of the obtained sample of very young protostars we used all objects within 500 pc which are properly classified as Class 0 or Class 0/1 to determine age and final star mass. Therefor we used three different evolutionary models for protostars from Smith (1998; 2000; 2002), Myers et al. (1998), and André et al. (2000). Considering the uncertainties in the measured source properties the predicted final star masses from the different models show a good correlation. The absolute ages are, however, very model dependent.

An investigation of the final star masses and the resulting mass function shows a good agreement with the IMF for stars with $M > 0.5\text{ }M_{\odot}$. Our obtained Class 0 sample is limited to sources with final masses above $0.4\text{ }M_{\odot}$. A number of objects (25 %) is found that possess a much lower luminosity than the rest of our sample, considering their bolometric temperature and envelope mass. These objects might be in a 'quiet' accretion phase or the time evolution of their mass accretion rate is significantly different from the majority. This might especially be the case in the Taurus star forming region, where all identified Class 0 or Class 0/1 sources belong to this group.

We are grateful to M. Rengel for providing a preprint of her paper. We thank the anonymous referee for very helpful comments and suggestions. M.D. Smith is acknowledged for providing the code of his evolutionary model and his comments. We thank M.P. Redman, T.P. Ray, and À. Gras-Velázquez for their help. This publication makes use of the Protostars Webpage hosted by the Dublin Institute for Advanced Studies. D. Froebrich received financial support by the Cosmo-Grid project, funded by the Program for Research in Third Level Institutions under the National Development Plan and with assistance from the European Regional Development Fund. This research has made use of the SIMBAD database, operated at CDS, Strasbourg, France. This research has made use of NASA's Astrophysics Data System. This publication makes use of data products from the Two Micron All Sky Survey, which is a joint project of the University of Massachusetts and the Infrared Processing and Analysis Center/California Institute of Technology, funded by the National Aeronautics and Space Administration and the National Science Foundation.

REFERENCES

André, P., Motte, F., Bacmann, A., 1999, *ApJ*, 513L, 57

André, P., Ward-Thompson, D., Barsony, M., 1993, *ApJ*, 406, 122

André, P., Ward-Thompson, D., Barsony, M., 2000, in *Protostars and Planets IV*, 59

Anglada, G., Rodríguez, L.F., 2002, *RMxAA*, 38, 13

Barsony, M., Kenyon, S.J., 1992, *ApJ*, 384L, 53

Bontemps, S., André, P., Kaas, A.A., Nordh, L., Olofsson, G., Huldtgren, M., Abergel, A., et al., 2001, *A&A*, 372, 173

Bontemps, S., André, P., Terebey, S., Cabrit, S., 1996, *A&A*, 311, 858

Bontemps, S., André, P., Ward-Thompson, D., 1995, *A&A*, 297, 98

Bourke, T.L., Garay, G., Lehtinen, K.K., Koehnenkamp, I., Launhardt, R., Nyman, L.-A., May, J., et al. 1997, *ApJ*, 476, 781

Cabrit, S., André, P., 1991, 379, 25

Calvet, N., Hartmann, L., Strom, S.E., 2000, in *Protostars and Planets IV*, 377

Carballo, R., Wesselius, P.R., Whittet, D.C.B., 1992, *A&A*, 262, 106

Cernicharo, J., Lefloch, B., Cox, P.; Cesarsky, D., Esteban, C., Yusef-Zadeh, F., Mendez, D. I., et al. 1998, *Science*, 282, 462

Chandler, C.J., Richer, J.S., 2000, *ApJ*, 530, 851

Chen, H., Grenfell, T.G., Myers, P.C., Hughes, J.D., 1997, *ApJ*, 478, 295

Chen, H., Myers, P.C., Ladd, E.F., Wood, D.O.S., 1995a, *ApJ*, 445, 377

Chini, R., Reipurth, B., Ward-Thompson, D., Bally, J., Nyman, L.-A., Sievers, A., Billawala, Y., 1997a, *ApJ*, 474L, 135

Chini, R., Reipurth, B., Sievers, A., Ward-Thompson, D., Haslam, C.G.T., Kreysa, E., Lemke, R., 1997b, *A&A*, 325, 542

Chini, R., Ward-Thompson, D., Kirk, J.M., Nielbock, M., Reipurth, B., Sievers, A., 2001, *A&A*, 369, 155

Clark, F.O., 1991, *ApJS*, 75, 611

Codella, C., Muders, D., 1997, *MNRAS*, 291, 337

Dame, T.M., Thaddeus, P., 1985, *ApJ*, 297, 751

Davis, C.J., Matthews, H.E., Ray, T.P., Dent, W.R.F., Richer, J.S., 1999, *MNRAS*, 309, 141

Dent, W.R.F., Matthews, H.E., Ward-Thompson, D., 1998, *MNRAS*, 301, 1049

Devine, D., Reipurth, B., Bally, J., 1999, *AJ*, 118, 972

Eiroa, C., Palacios, J., Casali, M.M., 1998, *A&A*, 335, 243

Eislöffel, J., Froebrich, D., Stanke, T., McCaughrean, M.J., 2003, 595, 259

Froebrich, D., Schmeja, S., Smith, M.D., Klessen, R.S., 2004, *A&A*, in prep.

Froebrich, D., Smith, M.D., Hodapp, K.W., Eislöffel, J., 2003, *MNRAS*, in press

Fuente, A., Neri, R., Martín-Pintado, J., Bachiller, R., Rodríguez-Franco, A., Palla, F., 2001, *A&A*, 366, 873

Giannini, T., Nisini, B., Lorenzetti, D., 2001, *ApJ*, 555, 40

Gibb, A.G., Davis, C.J., 1998, *MNRAS*, 298, 644

Gibb, A. G., Little, L.T., 2000, *MNRAS*, 313, 663

Gsten, R., 1994, in *The Cold Universe*, 169

Hartmann, L., 2002, *ApJ*, 578, 914

Henriksen, R., André, P., Bontemps, S., 1997, *A&A*, 323, 549

Holland, W.S., Greaves, J.S., Ward-Thompson, D., André, P., 1996, *A&A*, 309, 267

Huard, T.L., Sandell, G., Weintraub, D.A., 1999, *ApJ*, 526, 833

Hunter, T.R., Neugebauer, G., Benford, D.J., Matthews, K., Lis, D.C., Serabyn, E., Phillips, T.G., 1998, *ApJ*, 493L, 97

Hurt, R.L., Barsony, M., 1996, *ApJ*, 460, 45

Johnstone, D., Fich, M., Mitchell, G.F., Moriarty-Schieven, G., 2001, *ApJ*, 559, 307

Kalenskii, S.V., Promislov, V.G., Alakoz, A., Winnberg, A.V., Johansson, L.E.B., 2000, *A&A*, 354, 1036

Klessen, R.S., 2001, *ApJ*, 550, 77

Kun, M., Prusti, T., 1993, *A&A*, 272, 235

Ladd, E.F., Adams, F.C., Casey, S., Davidson, J.A., Fuller, G.A., Harper, D.A., Myers, P.C., Padman, R., 1991a, *ApJ*, 366, 203

Larson, R.B., 2003, *astro-ph*, 0306595

Launhardt, R., Henning, T., 1997, *A&A*, 326, 329

Launhardt, R., Mezger, P.G., Haslam, C.G.T., Kreysa, E., Lemke, R., Sievers, A., Zylka, R., 1996, *A&A*, 312, 569

Lehtinen, K., Haikala, L.K., Mattila, K., Lemke, D., 2001, *A&A*, 367, 311

Looney, L.W., Mundy, L.G., Welch, W.J., 2000, *ApJ*, 529, 477

Mardones, D., Myers, P.C., Tafalla, M., Wilner, D.J., Bachiller, R., Garay, G., 1997, *ApJ*, 489, 719

Mezger, P.G., Sievers, A.W., Haslam, C.G.T., Kreysa, E., Lemke, R., Mauersberger, R., Wilson, T.L., 1992a, *A&A*, 256, 631

Molinari, S., Testi, L., Brand, J., Cesaroni, R., Pallo, F., 1998, *ApJ*, 505L, 39

Moriarty-Schieven, G.H., Wannier, P.G., Keene, J., Tamura, M., 1994, *ApJ*, 436, 800

Moro-Martín, A., Noriega-Crespo, A., Molinari, S., Testi, L., Cernicharo, J., Sargent, A., 2001, *ApJ*, 555, 146

Motte, F., André, P., 2001, *A&A*, 365, 440

Myers, P.C., Adams, F.C., Chen, H., Schaff, E., 1998, *ApJ*, 492, 703

Nisini, B., Caratti o Garatti, A., Giannini, T., Lorenzetti, D., 2002, *A&A*, 393, 1035

O'Linger, J., Wolf-Chase, G., Barsony, M., Ward-Thompson, D., 1999, *ApJ*, 515, 696

Olmi, L., Felli, M., Cesaroni, R., 1997, *A&A*, 326, 373

Park, Y.-S., Kim, J., Minh, Y.C., 1999, *ApJ*, 520, 223

Persi, P., Ferrari-Toniolo, M., Marenzi, A.R., Anglada, G., Chini, R., Krügel, E., Sepúlveda, I., 1994, *A&A*, 282, 233

Persi, P., Marenzi, A.R., Gómez, M., Olofsson, G., 2001, *A&A*, 376, 907

Phillips, R.R., Gibb, A.G., Little, L.T., 2001, *MNRAS*, 326, 927

Prusti, T., Whittet, D.C.B., Assendorp, R., Wesselius, P.R., 1992a, *A&A*, 260, 151

Pudritz, R.E., Wilson, C.D., Carlstrom, J.E., Lay, O.P., Hills, R.E., Ward-Thompson, D., 1996, *ApJ*, 470L, 123

Rebull, L.M., Cole, D.M., Stapelfeldt, K.R., Werner, M.W., 2003, *AJ*, 125, 2568

Reipurth, B., Nyman, L.-A., Chini, R., 1996, *A&A*, 314, 258

Reipurth, B., Rodríguez, L.F., Chini, R., 1999, *AJ*, 118, 983

Rengel, M., Eislöffel, J., Hodapp, K.W., 2004, *A&A*, in prep.

Richer, J.S., Padman, R., Ward-Thompson, D., Hills, R.E., Harris, A.I., 1993, *MNRAS*, 262, 839

Rodríguez, L.F., Reipurth, B., 1996, *RMxAA*, 32, 27

Rodríguez, L.F., Gómez, Y., Reipurth, B., *ApJ*, 598, 1100

Sandell, G., Avery, L.W., Baas, F., Coulson, I., Dent, W.R.F., Friberg, P., Gear, W.P.K., Greaves, J., Holland, W., Jenness, T., et al., 1999, *ApJ*, 519, 236

Sandell, G., Knee, L.B.G., 2001, *ApJ*, 546L, 49

Sandell, G., Wright, M., Forster, J.R., 2003, *ApJ*, 590, 45

Saraceno, P., André, P., Ceccarelli, C., Griffin, M., Molinari, S., 1996, *A&A*, 309, 827

Schmeja, S., Klessen, R.S., 2004, *A&A*, 419, 405

Shirley, Y.L., Evans II, N.J., Rawlings, J.M.C., Gregersen, E.M., 2000, *ApJS*, 131, 249

Shu, F.H., Li, Z.-Y., Allen, A., 2004, *ApJ*, 601, 930

Smith M.D., 1998, *Ap&SS*, 261, 169

Smith, M.D., 2000, *IrAJ*, 27, 25

Smith, M.D., 2002, *The Origins of Stars and Planets: The VLT View*, J.Alves & M.McCaughrean (ed.)

Tafalla, M., Myers, P.C., Mardones, D., Bachiller, R., 1999, *A&A*, 348, 479

Thompson, M.A., Macdonald, G.H. , 2003, *A&A*, 407, 237

Visser, A.E., Richer, J.S., Chandler, C.J., 2002, *AJ*, 124, 2756

Vuong, M.H., Cambrésy, L., Epchtein, N., 2001, *A&A*, 379, 208

Wamsteker, W., 1981, *A&A*, 97, 329

Ward-Thompson, D., Buckley, H.D., 2001, *MNRAS*, 327, 955

Ward-Thompson, D., Eiroa, C., Casali, M.M., 1995b, *MNRAS*, 273L, 25

Wilner, D.J., Welch, W.J., Forster, J.R., 1995, *ApJ*, 449L, 73

Wolf-Chase, G., Moriarty-Schieven, G., Fich, M., Barsony, M., 2003, *MNRAS*, 344, 809

Young, C.H., Shirley, Y.L., Evans II, N.J., Rawlings, J.M.C., 2003, *ApJS*, 145, 111

Zinnecker, H., Bastien, P., Arcoragi, J.-P., Yorke, H.W., 1992, *A&A*, 265, 726

Table 1:: Obtained object parameters, sorted by SED quality

Object ^a	β	T _{bol}	L _{bol}	L _{smm} /L _{bol}	M _{env}	Class ^b
		[K]	[L _⊙]		[M _⊙]	
L 1448-I2	1.0	43	6.0	0.030	1.0	0/1 (ynn6)
L 1448 NW	2.1	<30	<2.8	>0.16	1.2	0 (yyy6)
L 1448 N	0.6	70	10	0.028	2.2	0/1 (ynn4)
L 1448 C	1.4	<60	8.3	0.029	1.1	0 (yyy6)
RNO 15 FIR	1.5	63	9.7	0.016	0.45	0/1 (ynn5)
RNO 15	1.5	<73	15	0.013	0.43	0 (yyy6)
NGC 1333 I1	1.9	<85	18	0.010	0.39	0/1 (?yy6)
IRAS 03256+3055	0.3	<61	1.0	0.043	0.34	0 [†] (yyy5)
NGC 1333-I2	1.4	<51	43	0.010	1.5	0 (yyy7)
NGC 1333-I4 A	0.3	<42	18	0.037	5.8	0 (yyy6)
NGC 1333-I4 B	1.2	<43	17	0.036	3.1	0 (yyy6)
IRAS 03282+3035	0.5	<63	1.3	0.062	0.73	0 (yyy5)
HH 211-MM	1.3	<33	3.6	0.046	0.80	0 (yyy6)
B 213	0.7	72	<0.39	<0.028	0.19	0/1 (ynn5)
IRAM 04191	0.6	<36	0.12	0.208	0.48	0 (yyy5)
L 1551-IRS 5	1.2	92	22	0.008	1.6	1 (ynn4)
L 1551-NE	0.5	91	4.2	0.009	0.57	1 (ynn5)
IRAS 04325+2402	1.4	73	0.97	0.057	0.52	0/1 (ynn4)
L 1527	1.6	56	1.9	0.056	0.80	0/1 (ynn4)
IRAS 05173-0555	1.0	<87	6.7	0.014	0.36	0/1 (?yy5)
RNO 43-MM	0.7	56	6.5	0.018	0.52	0/1 (ynn5)
OMC 3-MM 9	0.8	115	130	0.004	1.9	1 (nnn6)
OMC 3-MM 7	1.2	123	53	0.008	1.2	1 (ynn4)
L 1641 N	1.1	66	88	0.008	3.0	0/1 (ynn5)
HH 147 MMS	0.9	208	45	0.002	0.39	1 (nnn3)
HH 212-MM	1.0	<56	7.7	0.009	0.28	0 (yyy5)
HH 25 MMS	1.7	<41	7.2	0.063	1.2	0 (yyy5)
HH 111 MMS	0.9	78	23	0.010	1.0	0/1 (ynn5)
MonOB1 IRAS12 S1	1.3	41	76	0.045	5.5	0/1 (ynn5)
NGC 2264 G-VLA 2	1.1	<70	13	0.026	0.61	0 (yyy5)
IRAS 15398-3359	1.7	61	0.92	0.048	0.34	0/1 (ynn4)
IRAS 16293-2422	0.8	<41	21	0.019	4.6	0 (yyy7)
IRAS 16544-1604	1.0	<67	1.2	0.019	0.24	0 (yyy5)
IRAS 18148-0440	1.1	<54	10	0.010	0.70	0/1 (ynn5)
Serp-S68 N	1.4	<56	4.4	0.060	1.1	0 (yyy5)
Serp-FIRS 1	0.6	47	45	0.011	3.6	0/1 (ynn6)
Serp SMM 5	-0.6	113	3.6	0.018	1.4	1 (ynn4)
Serp-SMM 4	0.6	<62	5.2	0.028	1.5	0 (yyy6)
Serp-SMM 3	0.5	<65	4.9	0.019	1.0	0 (yyy5)
Serp-SMM 2	1.1	<75	4.0	0.012	0.36	0 (yyy5)
IRAS 18331-0035	1.8	48	4.4	0.057	0.72	0/1 (ynn4)
IRAS 18148-0440	1.1	95	3.3	0.040	0.67	1 (nnn3)
IRAS 19345+0727	1.2	<45	3.1	0.040	0.72	0 (yyy6)
IRAS 20050+2720	1.4	75	280	0.008	4.0	0/1 (ynn5)
IRAS 20386+6751	1.0	<42	8.4	0.033	1.2	0 (yyy5)
IRAS 21017+6742	1.5	73	0.86	0.050	0.18	0/1 (ynn5)
CB 230	1.0	69	7.7	0.022	0.56	0/1 (ynn4)
L 944-SMM 1	0.8	<80	4.7	0.035	0.44	0 (yyy5)
L 1251 B	0.2	83	9.0	0.023	2.1	1 (ynn4)
Cep E-MM	2.0	56	89	0.027	2.4	0 (yyy8)
L 1246-SMM 1	0.6	<95	6.6	0.044	0.96	0/1 (?yy5)

Continued on next page

Table 1 – continued from previous page

Object ^a	β	T _{bol} [K]	L _{bol} [L _⊙]	L _{smm} /L _{bol}	M _{env} [M _⊙]	Class ^b
IRAS 23238+7401	1.6	<61	0.78	0.038	0.16	0 (yyy5)
SVS 13 B MMS 1*	1.1	<163	<82	>0.004	1.2	? (??y4)
SVS 13 B MMS 2*	1.3	<165	<81	>0.003	1.1	? (??y4)
SVS 13 B MMS 3*	1.4	<169	<79	>0.002	0.42	? (??y4)
HH 114 MMS*	0.5	<84	<23	>0.013	1.4	0/1 (??y6)
OMC 3-MM 6*	0.7	<72	<100	>0.010	6.1	0 (yyy7)
NGC 2023-MM 1*	0.2	<87	200	0.002	2.8	? (ny7)
HH 24 MMS*	0.1	<78	<18	>0.019	2.7	0 (yyy5)
NGC 2068 LBS 17*	-0.7	<40	1.5	0.107	2.8	0 (yyy5)
IRAS 08076-3556*	0.0	117	>10	<0.009	1.1	1 (n?n5)
Ced 110 IRS 10*	—	36	0.38	0.063	—	0 [†] (yyy5)
Ced 110 IRS 4*	—	59	1.0	0.012	—	0/1 [†] (yn5)
BHR 71-MM*	—	68	7.9	0.008	—	0/1 [†] (yn5)
IRAS 12553-7651*	—	241	1.5	0.002	—	1 [†] (nnn3)
IRAS 13036-7644*	—	77	0.94	0.011	—	0 [†] (yyy5)
VLA 1623*	1.4	<59	<2.0	>0.052	0.80	0 (yyy7)
CB 232*	—	150	4.2	0.017	—	1 (yn4)
NGC 7129 FIRS 2*	0.9	72	330	0.011	8.6	0/1 (yn4)
L 1211*	1.7	191	62	0.005	0.28	1 [†] (yn4)
IRAS 23385+6053*	1.3	<54	19000	0.002	12	0/1 (ny7)
W3 OH**	4.5	—	—	—	190	—
L 1634 IRS 7**	1.5	—	—	—	0.60	—
HH 1-2 MMS 3**	1.7	—	—	—	0.31	—
HH 1-2 MMS 2**	2.3	—	—	—	0.19	—
L 1641-VLA 1**	0.8	—	—	—	1.6	—
L 1641 SMS III**	0.1	—	—	—	7.7	—
L 1641 SMS IV**	1.4	—	—	—	4.0	—
NGC 2024-FIR 5**	1.0	—	—	—	8.2	—
NGC 2024-FIR 6**	1.0	—	—	—	4.9	—
IRAS 12500-7658**	—	—	>0.62	—	—	—
IRAS 12533-7632**	—	—	>0.26	—	—	—
IRAS 12554-7635**	—	—	>0.17	—	—	—
IRAS 16017-3936**	—	—	>0.62	—	—	—
IRAS 16493-4242**	—	—	>4.8	—	—	—
HH 108 MMS**	1.2	—	—	—	0.49	—
G 34.24+0.13 MM**	0.9	—	—	—	2.8	—
R CrA R1**	—	—	>3.5	—	—	—
IRAS 19180+1114**	—	—	>5.2	—	—	—
S 106-SMM**	1.1	—	—	—	4.9	—
IC 1396 W**	—	—	>26	—	—	—
NGC 7538 S**	2.2	—	—	—	51	—

^a Object name used in this paper. Further common names are given in Table 3. The * markes objects where the SED is only well determined on one side of the peak and for the other side only upper limits or very few data is available. The ** markes objects with too few observational data to properly estimate even a limit for T_{bol}.

^b Classification due to the procedure described in Sect. 3.2. In brackets we give as 'y', 'n', or '?' the answers for our three different tests if the object is a Class 0 source. The ending number gives the orders of magnitude between the maximum of the emission and the NIR detection/upper limit.

[†] Classification uncertain, since non or no conclusive sub-mm or millimeter maps are available.

Table 2:: Age and Mass estimates from evolutionary models

Object ^a	Class ^b	Age ^c [10 ³ yrs]			M _{fin} ^c [M _⊙]		
		Smith	Myers	André	Smith	Myers	André
L 1448 NW	0 (yyy6)	23	75	5	0.2	0.8	1.2
L 1448 C	0 (yyy6)	37	225	8	0.4	1	1.1
RNO 15	0 (yyy6)	47	275	160	0.6	>2	2.0
IRAS 03256+3055	0 [†] (yyy5)	36	100	50	0.05	0.4	0.4
NGC 1333-I2	0 (yyy7)	33	300	4	2	>2	>3
NGC 1333-I4 A	0 (yyy6)	29	200	6	1	>2	>3
NGC 1333-I4 B	0 (yyy6)	29	200	6	1	>2	3.0
IRAS 03282+3035	0 (yyy5)	37	110	8	0.06	0.4	0.7
HH 211-MM	0 (yyy6)	25	75	8	0.3	0.8	0.8
IRAM 04191	0 (yyy5)	24	20	0	0.01	<0.3	0.5
OMC 3-MM 6*	0 (yyy7)	48	>500	8	5	>2	>3
HH 212-MM	0 (yyy5)	35	175	60	0.4	1	0.45
HH 25 MMS	0 (yyy5)	28	150	7	0.4	1	1.3
HH 24 MMS*	0 (yyy5)	53	300	6	0.8	>2	3.0
NGC 2068 LBS 17*	0 (yyy5)	27	75	0	0.10	0.4	2.5
NGC 2264 G-VLA 2	0 (yyy5)	44	250	25	0.6	>2	0.7
VLA 1623*	0 (yyy7)	36	150	6	0.1	0.5	0.9
IRAS 16293-2422	0 (yyy7)	29	200	5	1	>2	>3
IRAS 16544-1604	0 (yyy5)	39	150	10	0.06	0.4	0.3
Serp-S68 N	0 (yyy5)	35	150	6	0.2	0.8	1.1
Serp-SMM 4	0 (yyy6)	38	200	6	0.2	0.8	1.5
Serp-SMM 3	0 (yyy5)	40	200	8	0.2	0.8	1.0
Serp-SMM 2	0 (yyy5)	47	200	40	0.2	0.7	0.4
IRAS 19345+0727	0 (yyy6)	29	125	8	0.2	0.7	0.8
IRAS 20386+6751	0 (yyy5)	29	150	8	0.5	1.1	1.2
L 944-SMM 1	0 (yyy5)	53	200	18	0.21	0.7	0.5
Cep E-MM	0 (yyy8)	36	400	20	4	>2	2.8
IRAS 23238+7401	0 (yyy5)	36	100	20	0.04	0.4	<0.2
L 1448-I2	0/1 (ynyn6)	29	150	8	0.4	0.9	1.1
L 1448 N	0/1 (ynyn4)	44	250	6	0.4	1	2.1
RNO 15 FIR	0/1 (ynyn5)	39	225	30	0.4	1	0.7
NGC 1333 I1	0/1 (?yy6)	74	325	60	1	>2	0.8
B 213	0/1 (ynyn4)	41	90	5	0.01	<0.3	0.2
IRAS 04325+2402	0/1 (ynyn4)	43	150	30	0.04	0.4	0.7
L 1527	0/1 (ynyn4)	34	125	5	0.1	0.6	0.9
HH 114 MMS*	0/1 (?yy6)	70	350	10	1	>2	1.6
IRAS 05173-0555	0/1 (?yy5)	130	250	30	0.7	0.8	0.5
RNO 43-MM	0/1 (ynyn5)	35	200	20	0.3	0.9	0.6
L 1641 N	0/1 (ynyn5)	43	>500	9	4	>2	>3
HH 111 MMS	0/1 (ynyn5)	54	300	20	1	>2	1.2
MonOB1 IRAS12 S1	0/1 (ynyn5)	20	150	8	7.8	1.3	>3
IRAS 15398-3359	0/1 (ynyn4)	36	100	7	0.04	0.4	0.4
IRAS 18148-0440	0/1 (ynyn5)	34	200	20	0.5	1	0.8

Continued on next page

Table 2 – continued from previous page

Object ^a	Class ^b	Age ^c [10 ³ yrs]			M _{fin} ^c [M _⊙]		
		Smith	Myers	André	Smith	Myers	André
Serp-FIRS 1	0/1 (ynn6)	32	300	8	2	>2	>3
IRAS 18331-0035	0/1 (ynn4)	31	150	9	0.2	0.7	0.8
IRAS 20050+2720	0/1 (ynn5)	53	>500	10	10	>2	>3
IRAS 21017+6742	0/1 (ynn5)	43	125	40	0.04	0.4	<0.2
CB 230	0/1 (ynn4)	43	225	17	0.34	0.9	0.6
NGC 7129 FIRS 2*	0/1 (ynn4)	49	>500	8	14	>2	>3
L 1246-SMM 1	0/1 (?yy5)	290	275	8	1.93	0.8	1.0
IRAS 23385+6053*	0/1 (yny7)	36	>500	0	>50	>2	>3
L 1551-IRS 5	1 (ynn4)	290	350	9	6	>2	1.6
L 1551-NE	1 (ynn5)	250	225	10	1	0.7	0.7
OMC 3-MM 9	1 (nnn6)	370	>500	20	50	>2	2.8
OMC 3-MM 7	1 (ynn4)	380	>500	30	20	>2	1.7
HH 147 MMS	1 (nnn3)	430	>500	150	30	>2	2.0
IRAS 08076-3556*	1 (n?n5)	365	300	200	4.2	1.0	2.5
Serp SMM 5	1 (ynn4)	350	250	5	1	0.6	1.5
IRAS 18148-0440	1 (ynn3)	280	250	8	0.9	0.6	0.8
L 1251 B	1 [†] (ynn4)	61	250	7	0.4	1.0	2.0
L 1211*	1 (ynn4)	426	>500	8	33	>2	1.2

^a Object name used in this paper. Further common names are given in Table 3. The * marks objects where the SED is only well determined on one side of the peak and for the other side only upper limits or very few data is available.

^b Classification due to the procedure described in Sect. 3.2. In brackets we give as 'y', 'n', or '?' the answers for our three different tests if the object is a Class 0 source. The ending number gives the orders of magnitude between the maximum of the emission and the NIR detection/upper limit.

^c Ages and final masses obtained from the evolutionary models of Smith (1998; 2000; 2002), Myers et al. (1998), and André et al. (2000).

[†] Classification uncertain, since no or no conclusive sub-mm or millimeter maps are available.

A. Source Sample

Table 3:: Complete source sample

Object ^a	Ref. Obj. ^b	RA (2000)	Dec (2000)	Ref. ^c	d [pc]	Ref. ^c
W3 OH	15, 43	02 27 04.72	+61 52 24.7	71	2200	43
TW 3 (H ₂ O)						
L 1448-I2	22, 43	03 25 22.5	+30 45 06	59	300	54
IRAS 03222+3034						
L 1448 NW	48, 54, 70	03 25 35.65	+30 45 34.2	47	300	54
LDN 1448 IRS 3C						
L 1448 N	16, 22, 40, 43, 48, 54	03 25 36.3	+30 45 16	48	300	54
LDN 1448 IRS 3, IRAS 03225+3034						
L 1448 C	16, 22, 40, 43, 48, 54, 70	03 25 38.8	+30 44 00	48	300	54
L 1448-MM						
RNO 15 FIR	48, 64, 70	03 27 39.0	+30 12 59	71	350	70
LDN 1455 FIR						
RNO 15	70 (?)	03 27 42.9	+30 12 27	70	350	70
L 1455, B 204						
NGC 1333 I1	70 (Class0/1)	03 28 38.7	+31 13 32	71	350	54
IRAS 03255+3103						
IRAS 03256+3055	68 (Class1)	03 28 44.5	+31 05 39.7	68	400	2
NGC 1333-I2	40, 43, 54, 70	03 28 55.4	+31 14 35	58	350	54
IRAS 03258+3104						
SVS 13 B	22 (OF), 43, 48 (Class1), 49	03 29 03.06	+31 15 51.7	47	350	70
NGC 1333-I4 A	22, 40, 43, 54	03 29 12.04	+31 13 30.5	70	350	54
NGC 1333-I4 B	22, 43, 54	03 29 13.6	+31 13 06.6	70	350	54
IRAS 03282+3035	16, 43, 48, 54	03 31 20.3	+30 45 25	48	300	54
IC 348 MMS	63	03 43 56.9	+32 03 06	63	300	54
HH 211-MM	43, 54, 64, 70	03 43 56	+32 00 48	54	300	54
B 213	16 (OF), 48 (Class1), 54 (0/I), 68	04 19 43.00	+27 13 33.7	60	140	54
IRAS 04166+2706						
IRAM 04191	43, 54	04 21 56.9	+15 29 46	36	140	54
L 1551-IRS 5	13, 22 (OF)	04 31 34.15	+18 08 05.2	44	140	54
IRAS 04287+1801						
L 1551-NE	13, 22	04 31 44.44	+18 08 32	37	140	54
IRAS 04325+2402	26 (T _{bol} = 157 K)	04 35 35.0	+24 08 22	54	140	2
LDN 1535 IRS						
L 1527	13, 16, 43, 48, 49, 54	04 39 53.9	+26 03 11	48	140	54
IRAS 04368+2557						
HH 114 MMS	24, 43	05 18 15.21	+07 12 03	21	450	43
IRAS 05173-0555	70	05 19 48.9	-05 52 05	61	460	70
RNO 40 FIR, L 1634						
L 1634 IRS 7	70 (Class0?)	05 19 51.5	-05 52 06	70	460	70
RNO 43-MM	7, 43	05 32 19.4	+12 49 41	32	400	43
IRAS 05295+1247						
OMC 3-MM 6	25, 43	05 35 23.4	-05 01 29	41	450	43
OMC 3-MM 9	25	05 35 25.9	-05 05 44	41	450	43
OMC 3-MM 7	25	05 35 26.5	-05 03 55	41	450	43
IRAS 05329-0505						
HH 1-2 MMS 3	49	05 36 18.2	-06 45 45.3	49	460	49
L 1641 N	22 (OF), 70	05 36 18.6	-06 22 10	70	390	70
IRAS 05338-0624						
HH 1-2 MMS 2	49	05 36 18.8	-06 45 25.3	49	460	49
L 1641-VLA 1	43, 49	05 36 22.8	-06 46 07.6	49	460	49
HH 1-2 MMS 1						
L 1641 SMS III	70 (Class0/1)	05 36 24.0	-06 24 54	70	390	70
HH 147 MMS	49	05 36 25.2	-06 44 39.8	49	460	49

Continued on next page

Table 3 – continued from previous page

Object ^a	Ref. Obj. ^b	RA (2000)	Dec (2000)	Ref. ^c	d [pc]	Ref. ^c
IRAS 05339-0646						
L 1641 SMS IV	70 (Class0?)	05 36 41.8	-06 26 12	70	390	70
NGC 2023-MM 1	19, 43	05 41 24.54	-02 18 09	59	450	43
NGC 2024-FIR 5	6, 43	05 41 44.22	-01 55 41.32	65	450	43
NGC 2024-FIR 6	6, 43	05 41 45.17	-01 56 00.56	65	450	43
HH 212-MM	7, 43	05 43 51.1	-01 03 01	71	400	43
IRAS 05413-0104						
HH 25 MMS	12, 43	05 46 07.8	-00 13 41	52	450	43
HH 24 MMS	22, 43	05 46 08.8	-00 10 47	52	450	43
NGC 2068 LBS 17	45	05 46 30.8	-00 02 40	56	400	45
HH 111 MMS	49	05 51 46.3	+02 48 28	49	460	49
IRAS 05491+0247, LDN 1617 1						
MonOB1 IRAS12 S1	69	06 41 05.8	+09 34 09	69	800	69
NGC 2264 G-VLA 2	14, 43	06 41 10.9	+09 56 02	14	800	43
IRAS 06384+0958						
IRAS 08076-3556	11, 43	08 09 32.8	-36 05 00	71	400	43
BHR 12						
Ced 110 IRS 10	53	11 06 32	-77 23 42	20	150	53
Cha-MMS 1						
Ced 110 IRS 4	26, 53	11 06 47.14	-77 22 34.0	55	150	53
IRAS 11051-7706						
BHR 71-MM	23, 43	12 01 37	-65 08 54	71	200	43
IRAS 11590-6452						
IRAS 12500-7658	26	12 53 38.9	-77 15 53	57	180	6
IRAS 12533-7632	26	12 57 00.1	-76 48 35	52	180	6
IRAS 12553-7651	26	12 59 05.5	-77 07 34	71	180	30
IRAS 12554-7635	26	12 59 13.4	-76 51 11	71	180	6
IRAS 13036-7644	26, 43	13 07 36.0	-77 00 04.4	29	200	43
BHR 86						
IRAS 15398-3359	26, 48	15 43 01.3	-34 09 12	29	130	48
B 228						
IRAS 16017-3936	26	16 05 04.7	-39 45 04	71	130	26
VLA 1623	16, 22, 43	16 26 26.32	-24 24 30.1	47	160	43
IRAS 16293-2422	13, 16, 22, 43	16 32 22.8	-24 28 33	71	160	43
L 1689						
IRAS 16493-4242	26	16 52 56.6	-42 47 56	71	130	26
IRAS 16544-1604	39	16 57 19.5	-16 09 21	39	160	28
L 146, CB 68						
Trifid-TC 3	31, 43	18 02 07	-23 05 11	71	1680	43
IRAS 18148-0440	40, 43, 48, 54, 62	18 17 29.8	-04 39 38	71	200	54
L 483						
Serp-S68 N	18, 40, 43	18 29 48.1	+01 16 41	38	310	43
Serp-FIRS 1	18, 40, 43	18 29 49.79	+01 15 18.6	38	310	43
IRAS 18273+0113						
Serp SMM 5	40	18 29 51.1	+01 16 36	38	310	43
Serp-SMM 4	18, 40, 43	18 29 56.5	+01 13 10	38	310	43
Serp-SMM 3	18, 40, 43	18 29 59.2	+01 13 58	38	310	43
Serp-SMM 2	18, 40	18 30 00.2	+01 12 57	38	310	43
IRAS 18331-0035	40, 49	18 35 42.0	-00 33 18	71	310	24
HH 108/109 IRS, L 558						
HH 108 MMS	49	18 35 46.55	-00 32 41.8	71	310	24
G 34.24+0.13 MM	34, 43	18 53 21.4	+01 13 45.3	34	3700	43
R CrA R1	22	19 01 55.8	-36 57 29.6	22	130	22
IRAS 19156+1906	16, 40, 43, 48, 54	19 17 53.16	+19 12 16.6	71	300	54
L 723						
IRAS 19180+1114	40, 62	19 20 25.8	+11 19 52	71	300	3
L 673 A, RNO 109						

Continued on next page

Table 3 – continued from previous page

Object ^a	Ref. Obj. ^b	RA (2000)	Dec (2000)	Ref. ^c	d [pc]	Ref. ^c
IRAS 19345+0727 B 335, LDN 663	16, 22, 40, 43, 48, 54, 62	19 37 01.03	+07 34 10.9	71	250	54
IRAS 20050+2720 S 106-SMM	40, 49 9, 43	20 07 06.1 20 27 11.8	+27 28 59 +37 22 45	49 17	700 600	49 43
IRAS 20386+6751 L 1157	40, 43, 48, 49, 54, 64	20 39 06.5	+68 02 13	48	440	54
GF9-2	10, 43	20 51 30.1	+60 18 39	71	200	43
IRAS 21017+6742 L 1172	48, 62	21 02 23.1	+67 54 19	48	288	48
CB 230 IRAS 21169+6804, LDN 1177	68	21 17 40.0	+68 17 32	68	450	68
L 944-SMM 1	62	21 17 40.7	+43 18 08.5	62	700	1
IC 1396 W IRAS 21246+5743	64	21 26 06.1	+57 56 17	71	750	64
CB 232 IRAS 21352+4307	39	21 37 10.8	+43 20 39.4	39	350	27
NGC 7129 FIRS 2	33, 40	21 43 01.6	+66 03 26	50	1250	33
L 1251 B IRAS 22376+7455	68	22 38 42.52	+75 11 45.6	8	300	8
L 1211 IRAS 22451+6154	64	22 47 17.2	+62 02 34	42	725	64
Cep E-MM IRAS 23011+6126	43, 49, 64	23 03 13.1	+61 42 26	51	730	43
NGC 7538 S	66	23 13 44.98	+61 26 49.2	66	3500	46
L 1246-SMM 1	62	23 25 04.7	+63 36 40	62	730	62
IRAS 23238+7401 CB 244, LDN 1262 4	48, 62	23 25 46.4	+74 17 38	48	180	48
IRAS 23385+6053	35, 43	23 40 54.5	+61 10 28	67	4900	43

^a Object name used in this paper. Further common names are given below.

^b References where the object was mentioned as candidate or confirmed Class 0 source (in the samples listed in Sect. 2).

In brackets deviations from the general selection criteria are shown. In case the review article from André et al. (2000) provides the only reference, we additionally list the discovery paper of the source.

^c References for the origin of the position (Col. 5) and distance (Col. 7).

References: (1) Dame & Thaddeus (1985), (2) Clark (1991), (3) Ladd et al. (1991a), (4) Carballo et al. (1992), (5) Mezger et al. (1992a), (6) Prusti et al. (1992a), (7) Zinnecker et al. (1992), (8) Kun & Prusti (1993), (9) Richer et al. (1993), (10) Güsten (1994), (11) Persi et al. (1994), (12) Bontemps et al. (1995), (13) Chen et al. (1995a), (14) Ward-Thompson et al. (1995b), (15) Wilner et al. (1995), (16) Bontemps et al. (1996), (17) Holland et al. (1996), (18) Hurt et al. (1996), (19) Launhardt et al. (1996), (20) Reipurth et al. (1996), (21) Rodríguez & Reipurth (1996), (22) Saraceno et al. (1996), (23) Bourke et al. (1997), (24) Chini et al. (1997b), (25) Chini et al. (1997a), (26) Chen et al. (1997), (27) Codella & Muders (1997), (28) Launhardt & Henning (1997), (29) Mardones et al. (1997), (30) Olmi et al. (1997), (31) Cernicharo et al. (1998), (32) Dent et al. (1998), (33) Eiroa et al. (1998), (34) Hunter et al. (1998), (35) Molinari et al. (1998), (36) André et al. (1999), (37) Devine et al. (1999), (38) Davis et al. (1999), (39) Huard et al. (1999), (40) Park et al. (1999), (41) Reipurth et al. (1999), (42) Tafalla et al. (1999), (43) André et al. (2000), (44) Chandler & Richer (2000), (45) Gibb & Little (2000), (46) Kalenskii et al. (2000), (47) Looney et al. (2000), (48) Shirley et al. (2000), (49) Chini et al. (2001), (50) Fuente et al. (2001), (51) Giannini et al. (2001), (52) Johnstone et al. (2001), (53) Lehtinen et al. (2001), (54) Motte & André (2001), (55) Persi et al. (2001), (56) Phillips et al. (2001), (57) Young et al. (2001), (58) Ward-Thompson & Buckley (2001), (59) Anglada & Rodríguez (2002), (60) Hartmann (2002), (61) Nisini et al. (2002), (62) Visser et al. (2002), (63) Eislöffel et al. (2003), (64) Froebrich et al. (2003), (65) Rodríguez et al. (2003), (66) Sandell et al. (2003), (67) Thompson & Macdonald (2003), (68) Young et al. (2003), (69) Wolf-Chase et al. (2003), (70) Rengel et al. (2004), (71) SIMBAD database

B. Notes to individual objects

Table 4:: Notes to individual sources

Object ^a	Description
W3 OH	The 2MASS source is 3.5'' away from the coordinates adopted here.
L1448-I2	Fluxes from O'Linger et al. (1999) taken in the whole observed field are not used.
L 1448 NW	L 1448 NW is situated about 20'' NNW of the binary L 1448 N(A/B). The flux measurements are strongly influenced by the extended envelope of this nearby source. Fluxes from Chandler & Richer (2000) are given in Jy/beam and hence not used. The two 2.7 mm fluxes measured in small (<5'') apertures by Looney et al. (2000) are not used either.
L 1448 N	This source is actually a protostellar binary consisting of L 1448 IRAS 3A and IRAS 3B. Since IRAS 3A is about one order of magnitude brighter in the FIR as well as in the millimeter range, all the unresolved observations are attributed to IRAS 3A. Sub-mm fluxes taken in 40'' apertures (Shirley et al. (2000)) are not used due to the vicinity of L 1448 NW.
L 1448 C	We chose the values measured in boxes larger than 30'', in order not to miss emission from the outer regions of the extended envelope.
RNO 15 FIR	In the vicinity (about 1' south-east) of RNO 15 FIR the somewhat older source RNO 15 can be found. Both objects possess about the same brightness and hence flux measurements in large boxes might be influenced by RNO 15. This applies especially for the IRAS data. At 60 and 100 μ m there are discrepancies between the IRAS and ISO data. We used the ISO data since they are measured in a slightly smaller aperture.
RNO 15	The data at short wavelengths and around the maximum show a large scatter. This might partly be due to the nearby source RNO 15 FIR and also due to the fact that most of these measurements are taken before 1990 and suffer from large uncertainties.
NGC 1333 I1	Here the fluxes given by Sandell et al. (2001) are excluded. They are unreliable because the source is at the edge of their observed field.
IRAS 03256+3055	This source seems to consist of three objects (Young et al. (2003)). The IRAS position coincides with the weakest of the sub-mm sources. We excluded the fluxes measured in the 120'' apertures. There is a discrepancy between the 800 and 850 μ m point. We did not use the 800 μ m data from Anglada & Rodríguez (2002) since an unusual $\beta > 3$ would be obtained.
NGC 1333 I2	NGC 1333 I2 is a double source consisting of IRAS 2A and 2B with a separation of about 30''. IRAS 2A is much brighter than IRAS 2B in the sub-mm and hence the fluxes given for both objects are attributed to IRAS 2A.
SVS 13 B	Here it is particularly important to have the aperture sizes in which the photometry was obtained, since SVS 13 B is a triple protostellar system. It consists of MMS 1, 2, and 3. While MMS 1 and 2 have about the same brightness, MMS 3 is weaker. There are no data for the single sources at wavelengths shorter than 350 μ m.
NGC 1333 I4 A	This is a double source I4 A1 and I4 A2. I4 A1 is the brighter of the two sources and all the photometric data was attributed to this object.

Continued on next page

Table 4 – continued from previous page

Object ^a	Description
NGC 1333 I4 B	NGC 1333 I4 B is situated about 30'' south-east of NGC 1333 I4 A and hence the fluxes measured in large areas might be influenced. The data from Sandell et al. (2001) were taken in a relatively small aperture and might not include all the emission from the envelope. It was therefore not used. The flux from Rengel et al. (2004) is also excluded since the object is at the border of their map. The large fluxes given from Rebull et al. (2003) are not used since they might be influenced by surrounding emission.
IRAS 03282+3035	Even though this source seems to be isolated, the fluxes measured in the 120'' box by Sandell et al. (2000) are excluded.
HH 211 MM B 213	The data from Dent et al. (1998) are taken in an unknown aperture and hence not used. We did not use the fluxes measured in a 120'' aperture by Young et al. (2003) since they might be influenced by other surrounding sources. The IRAS 100 μ m limit was used as flux.
L 1551-IRS 5	Measurements taken in very small apertures (< 10'') were excluded. Also the data taken in the 270'' apertures are not used.
L 1551-NE	This object is a double source consisting of L 1551-NE A and B. All fluxes are attributed to L 1551-NE A.
IRAS 04325+2402	The measurements around 800 μ m and 1.3 mm do not correspond to each other. We did not use the low values given by Moriarty-Schieven et al. (1994), since very high values of β (> 3) are needed to explain these data. Also the upper limits given by Barsony & Kenyon (1992) seem to be too low in this context. The 2MASS source is 6'' away from the coordinates adopted here.
L 1527	There is a large scatter in the fluxes taken between 350 μ m and 1.3 mm even if they are taken with the same aperture size. We do not use data taken in the 120'' apertures. Difficulties occur since the IRAS points are only upper limits at all wavelengths. The 1.3 mm flux given by Chini et al. (1997b) for the whole observed field was excluded.
HH 114 MMS	There is a large scatter in the data at all wavelengths. We did not use the flux of the whole field given by Chini et al. (1997b). There are two sets of fluxes in the sub-mm data; low and high values. We chose the lower fluxes since they seem to present the better the central source and its envelope.
IRAS 05173-0555	The 2MASS source is 3'' away from the coordinates adopted here.
L 1634 IRS 7	The measurement from Chini et al. (1997b) at 1.3 mm for the whole field was excluded.
RNO 43-MM	No data shortward of 100 μ m are available. The 185 μ m point taken in a 3' aperture was not used. All the fluxes below 200 μ m seem to be anomalous due to the large apertures.
OMC 3-MM6	There is no IRAS detection. The 2MASS source is 6.6'' away from the coordinates adopted here.
OMC 3-MM9	The upper limit at 100 μ m in the IRAS catalogue seems to be too small compared to the other data. The 2MASS source is 3.5'' away from the coordinates adopted here.
OMC 3-MM7	The 2MASS source is 7'' away from the coordinates adopted here.
L 1641 N	There is a large scatter in the 1.3 mm data. We used only the flux measured in the 8.5'' aperture.
HH 1-2 MMS 2	The scatter in the measurements is very large. We did not use the huge 1.3 mm flux. The 2MASS source is 4.3'' away from the coordinates adopted here.
L 1641 VLA 1	

Continued on next page

Table 4 – continued from previous page

Object ^a	Description
L 1641 SMS III	The 2MASS source is 6.5'' away from the coordinates adopted here.
HH 147 MMS	Measurements taken in large apertures ($> 30''$) are excluded. The 2MASS source is 2.5'' away from the coordinates adopted here.
NGC 2023-MM 1	The 450 μ m point from Sandell et al. (1999) in the small aperture was excluded, as well as the data taken in the 180'' apertures.
NGC 2024-FIR 5	The huge 1.3 mm flux in the 30'' aperture was excluded.
HH 212-MM	The 1.3 mm flux from Chini et al. (1997b), measured in the whole observed field, was excluded.
HH 25 MMS	The two fluxes from Gibb & Davis (1998) measured in large apertures at 60 and 100 μ m are excluded. The 1.3 mm point is not used.
HH 24 MMS	All the IRAS points are just upper limits. The 1.3 mm flux from Launhard et al. (1996) measured in a 30'' aperture was excluded.
NGC 2068 LBS 17	All data shortward of 100 μ m are upper limits.
HH 111 MMS	The data obtained in large apertures ($\geq 30''$) were excluded as well as the high flux at 1.3 mm. The 2MASS source is 4'' away from the coordinates adopted here.
MonOB1 IRAS12 S1	The 2MASS source is 4'' away from the coordinates adopted here.
IRAS 08076-3556	The 2MASS source is 4.7'' away from the coordinates adopted here.
BHR 71-MM	The 2MASS source is 4'' away from the coordinates adopted here.
IRAS 12553-7651	The 2MASS source is 7'' away from the coordinates adopted here.
IRAS 15398-3359	The measurements in the 120'' apertures are excluded. The 2MASS source is 3'' away from the coordinates adopted here.
IRAS 16017-3936	The 2MASS source is 9'' away from the coordinates adopted here.
VLA 1623	This source is a double object consisting of the two sources VLA 1623 A and B, which are comparably bright in the millimeter range. The measurements from Pudritz et al. (1996) were excluded.
IRAS 16293-2422	IRAS 16293-2422 consists of two sources, IRAS 16293 A and B, separated by about 4'' (Looney et al. (2000)). We used only the data given for both objects together.
IRAS 16493-4242	The 2MASS source is 3.5'' away from the coordinates adopted here.
IRAS 18148-0440	The data taken in the 19 and 120'' apertures are excluded. The 2MASS source is 6'' away from the coordinates adopted here.
Serp SMM 5	The 2MASS source is 4'' away from the coordinates adopted here.
Serp SMM 3	The flux at 3.4 mm measured in the small aperture was not used.
Serp SMM 2	The upper limits at long wavelengths are taken within small apertures and hence do not contradict the fluxes.
IRAS 18331-0035	The 1.3 mm flux taken in a 11'' aperture was excluded. The 2MASS source is 3'' away from the coordinates adopted here.
HH 108 MMS	The 1.3 mm flux taken in a 11'' aperture was excluded.
G 34.24+0.13 MM	The 2MASS source is 5'' away from the coordinates adopted here.
IRAS 19156+1906	The large flux at 1.3 mm given by Cabrit & André (1991) was excluded. Also all data taken in apertures larger than 100'', as well as the other large flux taken at 1.3 mm were not used.
IRAS 19180+1114	The 2MASS source is 3'' away from the coordinates adopted here.
R CrA R1	The 2MASS source is 5'' away from the coordinates adopted here.
IRAS 19345+0727	IRAS 19345+0727 shows a large scatter in the sub-mm fluxes. We did not use the data taken in apertures larger than 120''.

Continued on next page

Table 4 – continued from previous page

Object ^a	Description
IRAS 20050+2720	The 2MASS source is $2.5''$ away from the coordinates adopted here.
IRAS 20386+6751	The sub-mm data taken in apertures larger than $60''$ were excluded. There is large scatter in the sub-mm data.
IRAS 21017+6742	Sub-mm fluxes measured in the $120''$ apertures are excluded. There is a large scatter in the sub-mm data.
CB 230	The 2MASS source is $2''$ away from the coordinates adopted here.
L 944-SMM 1	The sub-mm fluxes measured in the $50''$ apertures by Visser et al. (2002) are used.
IC 1396 W	The IRAS data might be confused by other cold dust in the vicinity.
CB 232	This is a double source consisting of CB 232 SMM 1 and SMM 2. SMM 1 is much brighter in the sub-mm. Hence, all data are attributed to this object. The 2MASS source is $6''$ away from the coordinates adopted here.
NGC 7129 FIRS 2	From the 1.3 mm points we chose the 1.49 Jy, since all the others contradict significantly with the data taken at nearby wavelengths.
L 1251 B	Data taken in the $120''$ apertures are excluded.
L 1211	These are several (at least four) sources. Also there are no sub-mm data. The ISO data represent the object MMS 4, while the IRAS source might include all objects (MMS 1, 2, 3, and 4). The ISO data were used and the IRAS points are excluded. The 2MASS source is $6''$ away from the coordinates adopted here.
Cep E-MM	This is a double source with a separation of $1.4''$. The flux of Moro-Martín et al. (2001) at 1.3 mm is not used due to the small aperture.
NGC 7538 S	The 2MASS source is $3''$ away from the coordinates adopted here.
L 1246-SMM 1	The sub-mm fluxes taken in the $50''$ apertures by Visser et al. (2002) are used.
IRAS 23238+7401	The $120''$ aperture measurements are excluded.

^a Object name used in this paper. Further common names are given in Table 3.